JACS
JOURNAL OF THE AMERICAN CHEMICAL SOCIETY

Article

pubs.acs.org/JACS

Transient Porosity in Densely Packed Crystalline Carbazole–(*p*-Diethynylphenylene)–Carbazole Rotors: CO_2 and Acetone Sorption Properties

Andrés Aguilar-Granda,[†] Salvador Pérez-Estrada,[∥] Elí Sánchez-González,[‡] J. Raziel Álvarez,[‡] Joelis Rodríguez-Hernández,[⊥] Mario Rodríguez,[#] Arian E. Roa,[†] Simón Hernández-Ortega,[†] Ilich A. Ibarra,[‡] and Braulio Rodríguez-Molina*[,†]

[†]Instituto de Química, [‡]Laboratorio de Fisicoquímica y Reactividad de Superficies (LaFReS), Instituto Investigaciones en Materiales, Universidad Nacional Autónoma de México, Del. Coyoacán, 04510 Ciudad de México, México

[∥]Department of Chemistry and Biochemistry, University of California, Los Angeles, California 90095, United States

[⊥]Centro de Investigación en Química Aplicada (CIQA), Blvd. Enrique Reyna Hermosillo, No. 140, Saltillo, Coahuila 25294, México

[#]Centro de Investigaciones en Óptica, A.P. 1-948, León, Guanajuato 37000, México

Supporting Information

ABSTRACT: We report for the first time the high sorption properties of a molecular rotor with no permanent voids or channels in its crystal structure. Such crystalline phase originates from THF, DCM, or the irreversible desolvation of entrapped benzene molecules. From these, the benzene in its solvate form acts as rotation stopper, as supported by dynamic characterization using solid-state ^{2}H NMR experiments. In the solvent-free form, the diffusion of small quantities of iodine vapors caused a significant change in the intramolecular rotation, increasing the known activation energy to rotation from 8.5 to 10.6 kcal mol^{-1}. Notably, those results paved the way for the discovery of the high CO_2 uptake (201.6 cm^3 g^{-1} at 196 K, under 1 atm) and acetone (5 wt %), a sorption property that was attributed to both, the restriction of the molecular rotation at low temperatures and the flexibility of the molecular axle made of conjugated *p*-(ethynylphenylene), surrounded by carbazole.

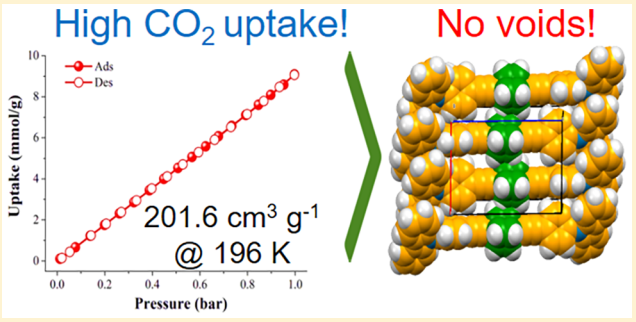

INTRODUCTION

Carbon dioxide emissions generate the unwanted greenhouse gas effect[1] which is the main gas responsible for global warming. Therefore, a considerable reduction of the CO_2 emissions is crucial to limit the increase in average global temperature (below 275 K).[2] To address this issue, numerous porous materials with increasingly larger gas uptakes have been developed.[3] Among them, porous organic materials[4] have gained considerable attention as an alternative to metal–organic frameworks.[5] They have numerous possible applications, among them gas storage,[6] molecular separation,[7] and catalysis.[8] Interestingly, the term "porous" in these materials has evolved thanks to the interesting sorption properties found in molecular crystals: from the early requirement of well-defined channels within the crystals,[9] to the current opinion that the presence of internal, interstitial, or latent voids are a prerequisite of the material to be considered porous.[10]

Depending on the nature of those voids, the porosity of these materials could be classified as intrinsic or extrinsic. For example, molecular cages are tailored solids that feature intrinsic porosity, which have been successively improved to show excellent sorption properties, though producing crystalline cages remains a great challenge.[11] However, crystalline solids with extrinsic porosity can result from molecules that form channels, like tris(*o*-phenylenedioxy)cyclophosphazene,[12] or by desolvation of the entrapped solvent molecules in calixarenes.[13] In the latter cases, the resulting pores are not evidently interconnected, so the observed gas sorption has been attributed to the cooperative internal motion of the molecules, resulting in a collective process that enables a better diffusion process.[14] Unfortunately, not many molecules crystallize in a channel-forming manner, nor is the desolvation route always a good strategy because it may render amorphous solids with reduced sorption properties.

The study and control of collective internal motion in crystalline solids is exactly the main goal in the field of molecular rotors.[15] Particularly, it has been reported that when the rotors are embedded in porous scaffolds, the diffusion of a guest into the framework could modify the motion of the rotary component, and this could be used as a reliable internal probe of the interaction.[16] On the basis of this idea, some research

Received: February 27, 2017
Published: May 14, 2017

DOI: 10.1021/jacs.7b02015
J. Am. Chem. Soc. 2017, 139, 7549–7557

groups have successfully incorporated mobile parts in permanently porous metal−organic frameworks (MOFs),[17] periodic mesoporous organosilicas (PMOs),[18] or polymers of intrinsic porosity (PIMs),[19] among other porous materials.[20] Due to the vast number of these networks, this remains a fertile area for dynamic characterization but is hampered when the materials do not show internal motion due to the pore size or if the guest−host interaction is not detectable. In addition, some known complications of these materials, i.e., the low stability of some MOFs (challenging when working in humid conditions) or the low crystallinity of PMOs (difficult structure−function correlation), make it highly desirable to find crystalline, discrete organic compounds that feature both selective porosity and molecular motion.

This is precisely the strategy we envisioned as an alternative approach. That is, we would like to start with organic crystalline rotors, since they contain the structural elements that facilitate the intramolecular motion, and progressively fine-tune the structures with appropriate functional groups to enable the uptake of certain chemical species. Although our strategy is still in early stages, we were encouraged by the elegant work of the Sozzani group. We considered that our recently reported molecular rotor **1**,[21] which shows a 6 MHz rotation frequency at room temperature, could be a useful structural platform for more elaborated structures with possible sorption properties. Therefore, we carried out proper control studies to obtain reference values for future compounds. Surprisingly, after solid-state experiments and physicochemical measurements, we found that this rotor shows an intriguing porosity that we termed "transient", since the crystal structure has no internal voids and its sorption is triggered only by certain external stimulus, thus challenging the notion that a void is a prerequisite.

In this manuscript, we first describe how the internal motion of rotor **1**, studied by variable-temperature solid-state ^{2}H NMR, has been proved to be sensitive to some chemical species. We start by describing the rotation of the molecular components in its known benzene solvate (form I), and we compared them to that of its the thermally stable solvent-free crystal reported earlier (form II). The two types of motion, before and after the desolvation, helped us to discriminate the significant influence in the intramolecular motion of small quantities of benzene and iodine vapors diffused into the solvent-free crystals (Figure 1). From these, the iodine vapors significantly restrict the motion of the rotor, increasing the activation barrier to rotation by 2 kcal/mol, as compared to that of the nontreated sample. These experiments opened the door to N_2, CO_2, and several VOCs sorption experiments, showing high uptakes of CO_2 (39.6 wt % at 196 K, under 1 atm) and acetone (5.4 wt %). Considering that the X-ray crystal structure of **1**, obtained from synchrotron radiation, does not feature channels or voids, the uptake was attributed to the lack of intramolecular rotation and the flexibility of the central *p*-(ethynylphenylene) axle, which allows the formation of transient, selective pores.

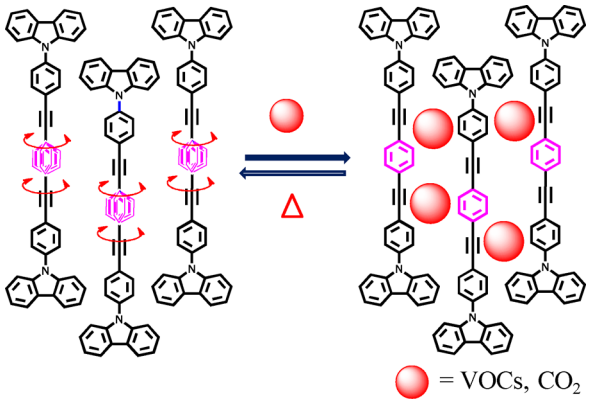

Figure 1. Changes in the rotational behavior of carbazole-based molecular rotor **1** reported here, upon the diffusion of external stimulus (VOCs = volatile organic compounds).

RESULTS AND DISCUSSION

Intramolecular Dynamics of Phase I. While we have demonstrated in an earlier report that the central phenylene is the only mobile component in the solvent-free crystal, in the case of the solvate, the entrapped benzene should be recognized as an additional rotary constituent. Thus, dynamic characterization was carried out to determine how its presence within the crystal affects the behavior of the phenylene. An approach to probe only the potentially mobile components in the solvate was to carry out solid-state deuterium NMR experiments. This nucleus is widely used to identify internal dynamics in solid-state materials, due to the high sensitivity of the C−D bond to the geometry and rate of the motion; thus, if the deuterated molecular component undergoes a motion with a rotational frequency within 10^4−10^8 Hz, then it would be reflected in the deuterium spectrum.[22,23]

The motion of benzene molecules in the solvate was studied by carrying out a crystallization of compound **1** in deuterated benzene. This strategy enabled us with the unique opportunity to capture the onset of the crystallization process,[24] by using a glass tube with a supersaturated solution of **1** in benzene-d_6 and acquiring different ^{2}H spectra at room temperature (Figure S14). At the beginning of the crystallization, only a large isotropic signal was detected in the spectrum, reflecting that the deuterated solvent is moving freely. The gradual crystallization and the gentle removal of the excess of solvent caused a gradual transformation of the ^{2}H line shape until two distinguishable shoulders with a distance between peaks of 62 kHz became dominant. The anisotropy of the line shape and the corresponding simulation revealed that the benzene-d_6 experiences a fast in-plane rotation (60° jumps or 6-fold rotation) when it crystallizes in between two molecules of **1** (Figure 2b). A similar rotational behavior has been reported before in other host−guest complexes.[25] Notably, if the temperature of the sample is raised only ten degrees, i.e., to 305 K, then an isotropic signal appears again in the spectrum, consistent with the escape of the benzene at the beginning of the desolvation and the phase transition. Finally, the lack of the signal in the spectrum evidenced the complete removal of benzene from the lattice at 315 K or higher (Figure S14).

A complementary view of this process was achieved by using the compound that contains a deuterated central 1,4-diethynylphenylene (**1**-d_4), crystallized from regular benzene. At the beginning of this experiment, two types of signals were observed, that is, one isotropic peak from the fully dissolved compound **1**-d_4 tumbling around freely and a characteristic Pake pattern with two singularities separated by 132 kHz; these indicate that upon crystallization the central ring of compound **1** does no longer experiences free motion but is restricted to oscillations with very low frequency (10^4 Hz) as illustrated in Figures 2 and S15. Heating the sample to 323 K caused a full desolvation of the sample, enabling the fast 180° rotation

DOI: 10.1021/jacs.7b02015
J. Am. Chem. Soc. 2017, 139, 7549−7557

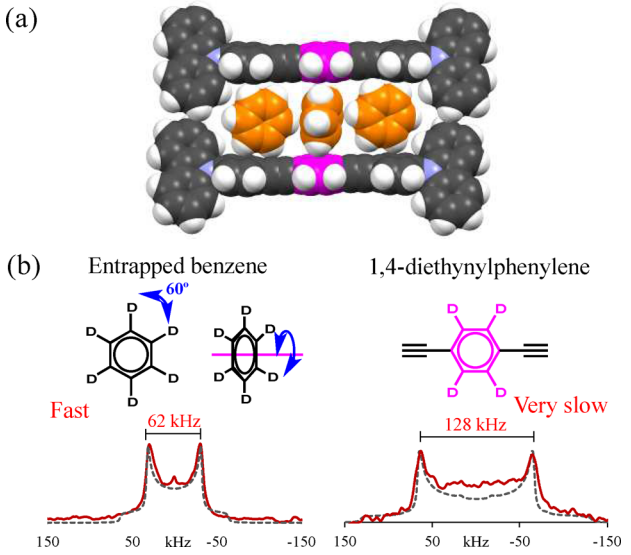

Figure 2. (a) Section of the crystal array of the benzene solvate of **1**. (b) ^{2}H wide-line spectra of the fast in-plane 6-fold rotation of benzene molecules and the very slow motion of the 1,4-diethynylphenylene fragment.

reported before (see Figure S15). In addition, HSM experiments helped us to assess the phase transition in a more controlled manner (Figure S29). The loss of solvent in **1** resulted in the generation of a crystalline powder, although this is not necessarily the case in other solvates that can render amorphous solids.[26]

X-ray Structure of Solvent-Free Form II by Synchrotron Radiation. Besides the benzene desolvation that produces the solvent-free crystals of compound **1** (form II), such form can also be accessed from evaporation of dichloromethane or tetrahydrofuran solutions. After various unsuccessful attempts to grow large single crystals using these solvents and traditional methods, we resorted to the less explored gel-assisted crystallization method.[27] This approach reduces the rate of crystallization by regulating the diffusion of a saturated solution through a tridimensional organic network, i.e., poly(ethylene) oxide.[28] This method provided larger needles that were successfully collected by X-ray diffraction using Cu $K\alpha$ radiation (three-day experiment) or synchrotron radiation. In both experiments the same structure was obtained, but the best crystallographic results evidently came from the synchrotron source and were selected for a detailed analysis. The crystallographic data for compound **1** is available in the Supporting Information and from the The Cambridge Crystallographic Data Centre (CCDC deposit number 1534257) free of charge via www.ccdc.cam.ac.uk/data_request/cif.

The crystal structure was solved in the triclinic system in the space group $P\bar{1}$, showing two disordered positions of the central phenylene ring with a 50:50 occupancy, related by an angular displacement of ca. 75° (Figure 3a).[29] Relevant crystallographic parameters of the newly obtained form I along with those of previously reported form II are compiled in Table S1. Interestingly, besides the disorder in the central aromatic ring, no significant changes in the molecular conformation were observed with respect to the molecules in the solvate, which can be visualized as if the molecules were rigid rods piling up after the benzene escapes the lattice. One large difference is that in form II, only two phenylene rings remain coplanar and the third is out-of-plane compared to its fully coplanar conformation in the solvate (Figure S1). Interestingly, the crystal array shows a very dense columnar stack with numerous CH···π interactions among neighboring molecules, a packing that resembles a cogwheel of the macroscopic world and which fully supports our earlier findings of rapid internal motion in **1** (Figure 3b).

Diffusion of Benzene and Iodine Vapors in Form II. After establishing the rotation of the molecular components in the benzene solvate of **1**, we explored if the phase transition was reversible from solvent-free to solvate; in this case, it should be reflected in the internal motion. To this end, recently desolvated crystals were exposed to benzene vapors on a glass plate in a closed vial. After 12 h, the crystals were analyzed under the optical microscope, at which time we noticed that the

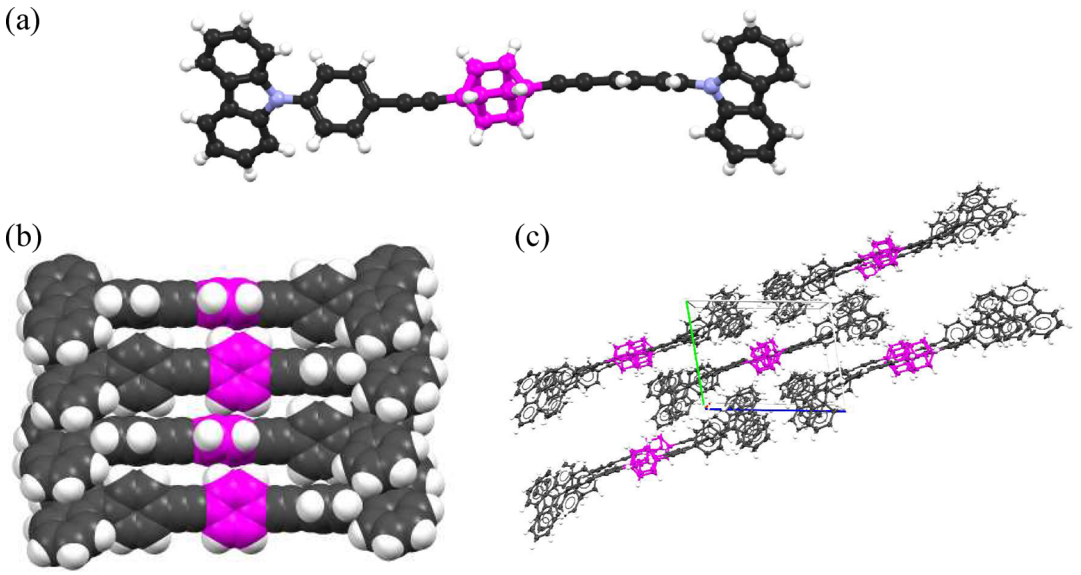

Figure 3. (a) Molecular structure of rotor **1** from synchrotron radiation. (b) Dense packing of **1** along one column, with no significant voids. (c) View down the *a*-axis of the columnar array.

DOI: 10.1021/jacs.7b02015
J. Am. Chem. Soc. 2017, 139, 7549−7557

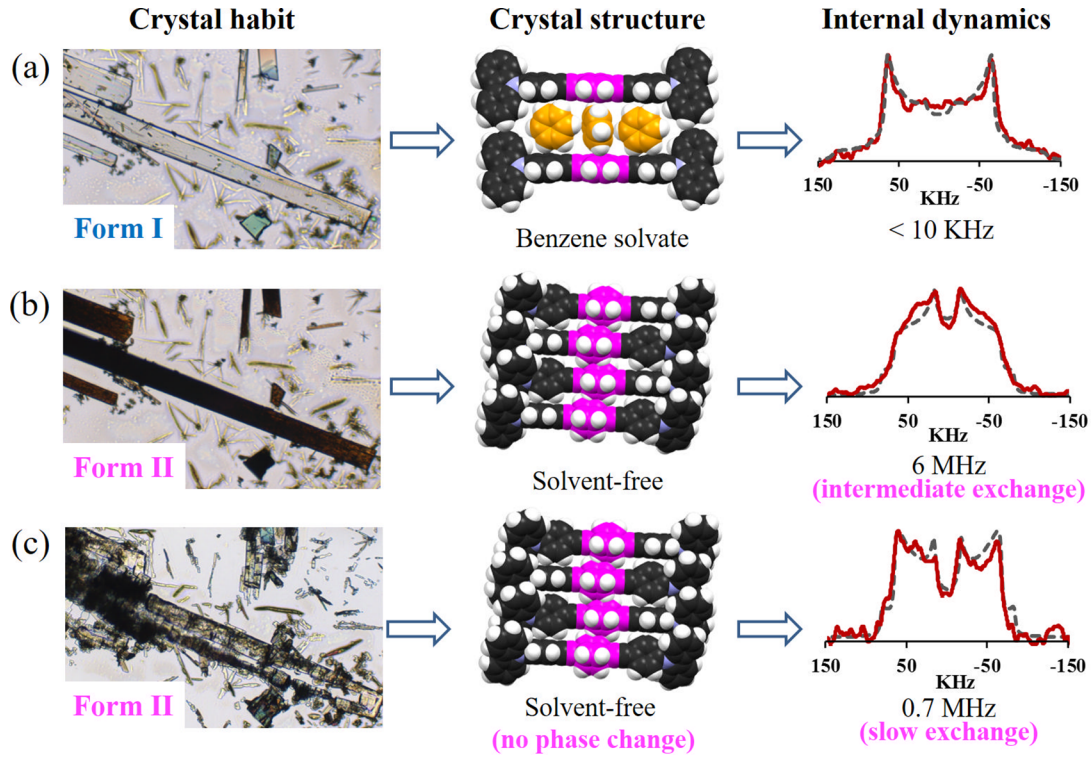

Figure 4. Overview of the changes in crystalline compound **1**. Columns: crystal habits (left), associated molecular structures (middle), and their corresponding internal rotation (right). Rows: (a) freshly crystallized solvate prisms where the entrapped benzene restricts the intramolecular motion, (b) solvent-free form obtained by heating the previous benzene-solvate, with rotation in the intermediate exchange, and (c) same solvent-free crystals exposed to benzene vapors (12 h), recovered some birefringence without changing the crystal phase but showed reduced rotation.

crystals were no longer opaque. Motivated by these results, the exposure was carried out using deuterated analog **1**-d_4 to determine if the benzene solvate was restored. Remarkably, the deuterium spectrum of the exposed sample was significantly different when compared with those from the solvate or the solvent-free form (Figure 4).

The experimental ^{2}H spectrum of the treated sample was best fitted when considering that the central 1,4-diethynylphenylene-d_4 undergoes 180° jumps (2-fold flips) at a frequency of 0.70 MHz (Figure S17), confirming that some amount of benzene vapors was allowed back into the crystal lattice, without completely stopping the intramolecular rotation. Surprisingly, the PXRD pattern of this same sample showed exclusively the solvent-free phase II, with no traces of phase I. Nevertheless, a Le Bail fitting of the powder data (Table S2) revealed that the volume of the unit cell increases its size slightly, from 1572.12(2) to 1590.58(6) Å^3, suggesting that a small amount of benzene could be diffused inside the crystal. Physicochemical studies detailed below showed that only a very small amount of benzene returns to the crystals and that minor quantity is the responsible of the changes in the intramolecular rotation.

Motivated by this result, we posed the hypothesis that this material could display sorption properties. To this end, we decided to evaluate the behavior of the solvent-free phase II using other chemical species. We decided to conduct an experiment reported by the Sozzani group,[16] exposing a microcrystalline sample of solvent-free **1**-d_4 to vapors of iodine for 12 h, during which the sample turned reddish-brown. Gratifyingly, the resulting deuterium line shape is analogous to the one obtained after exposition to benzene vapors, that is, the rotational frequency of **1** at room temperature was reduced from 6 MHz down to ca. 0.75 MHz.

From the thermodynamic parameters of activation (entalphy and entropy) of the untreated sample, it can be concluded that the rotation in compound **1** is not correlated, that is, the motion of each rotor inside the crystal is independent. With that in mind, we considered that a uniform slowdown of the intramolecular rotation upon vapors exposure can be considered as evidence of the presence of a small amount of I_2 inside the crystals.

Indeed, such chemical stimulus needed to be determined to further support our results. To ensure this, four additional studies were carried out: (1) powder X-ray diffraction (PXRD), (2) electron paramagnetic resonance (EPR), (3) X-ray fluorescence (XRF), and (4) variable-temperature ^{13}C CPMAS, as detailed below.

The PXRD results evidenced that the crystal structure does not significantly change upon exposure to iodine vapors, and no additional peaks were detected in the X-ray diffraction pattern (Figure S5). However, the Le Bail adjustment of the X-ray data reveals that the crystal lattice expands slightly upon treatment compared to that of the untreated sample from 1572.12(2) to 1596.78(2) Å^3 along with small elongation of the lattice parameters and change in its angles as detailed in Table S2. The absence of new peaks in the difractrogram could be indicative that iodine is not located in a periodic manner but randomly diffused instead.

Moreover, EPR experiments clearly corroborated that the iodine (I_2) is incorporated into the crystals of **1** and that electrons are transferred from the rotor to iodine creating a charge-transfer complex between the I_2 and the rotor which facilitates the creation of holes as indicated by the Lorentzian

DOI: 10.1021/jacs.7b02015
J. Am. Chem. Soc. 2017, 139, 7549−7557

line centered at g = 2.0048 with a peak-to-peak line width ΔH_{pp} of ca. 10 G (Figures S9–S11); this is consistent with several reports of iodine-doped crystals of pentacene.[30]

Additionally, we carried out XRF experiments[31] to undoubtedly show the presence of iodine in the crystalline samples of rotor **1**. According with these experiments, the pristine sample showed minimum traces of copper, palladium, and iodide coming from the cross-coupling reaction. When compared to the iodine-treated samples, there was an increase of about a factor of 10 in the L line of iodine as well as an increase of about a factor of 14.7 in the K line of iodine (Figure S8). The relatively high amount of iodine could be due to the superficial and diffused iodine.

Finally, solid-state NMR ^{13}C CPMAS also supported the presence of iodine, by comparing the spectrum with that of the nontreated sample. We observed changes in the intensity of the signals associated with the central phenylene and the alkyne fragments, ca. 130 and 108 ppm, respectively, suggesting that iodine is nearby the central part of the molecule, affecting the ^{1}H → ^{13}C cross-polarization (Figure S12). We also carried out variable-temperature ^{13}C CPMAS experiments at 175, 295, and 375 K, and no significant changes were found, thus ruling out that the changes in the spectrum are due to chemical exchange of inequivalent carbons (Figure S13).

These results strongly suggested that the crystals of **1** allow the diffusion of a small amount of iodine vapors without undergoing a solid-to-solid phase transition; however, contrary to the labile benzene solvate, the I_2–phenylene interaction[32] has been reported to be more persistent than the benzene–phenylene interaction. Qualitatively speaking, the reddish color of the sample was preserved for several hours or even days, indicating that the I_2 remained longer within the crystals.

Because of the longer persistence of I_2, a treated sample was used to acquire ^{2}H experiments at different temperatures from 265 K up to 325 K. The line shape fitting analyses revealed that the central 1,4-phenylene still experiences 180° rotations even with I_2, as it occurred in the nontreated sample, but this time it must surpass a higher barrier to rotation (E_a= 10.6 kcal/mol), 2 kcal/mol more than that reported earlier for the solvent-free form, as illustrated in Figure 5, as a reference.

More importantly, the correlation between experimental and simulated data allowed the construction of an Eyring plot (Figure S19), to extract the enthalpy and entropy components of the processes (Table 1). The activation enthalpy $\Delta H^{‡}$ from the iodine-treated sample is higher than that from the solvent-free from, which is consistent with the values of the activation energy to rotation. Interestingly, the entropy in the treated sample is larger than that of the solvent-free form. These results were interpreted as an evidence of the interaction between iodine and the central phenylene, making a more disordered transition state.

Considering all these results together, it became evident that the solvent-free phase of compound **1** can accommodate small amounts of chemical vapors within the crystals, i.e., benzene or iodine, both of which reduce the intramolecular rotation frequency without altering the crystallographic phase. Subsequently, we resorted to typical physicochemical measurements to explore in deep this behavior with other gases, as detailed below.

Transient Porosity of the Form II of Compound 1. As detailed in the Introduction, some discrete organic molecules have been reported as porous after the removal of encapsulated solvent molecules if the desolvation leaves empty cavities in the lattice, thus enabling several potential applications of the solids. However, according with the X-ray studies, the solvent-free form of compound **1** has a high density with no detectable voids, so it could be reasonable to say that porosity should not be expected. Nevertheless, the interesting results from solid-state NMR motivated us to carry out sorption experiments, starting with N_2 at 77 K. To this end, we used a sample of **1**, in its solvent-free form II, activated under mild conditions at 353 K and 10^{-5} bar for only 30 min. We rationalized that these mild outgassing conditions were appropriate since this material should not be as rigid as zeolites or metal–organic frameworks (MOFs) and that perhaps higher temperatures and/or longer activation times could promote sample degradation. The activated sample of **1** was cooled down to 77 K, and a N_2 adsorption–desorption measurement was recorded. The very low N_2 uptake and the shape of the isotherm (nonporous, see Figure S22) confirmed that compound **1** does not have permanent pores. Importantly, the sample retained its crystallinity after the activation and the N_2 adsorption–desorption isotherm. Since the crystallinity was indeed retained, the very low N_2 uptake could be attributed to the poor selectivity for N_2.

Complementary investigations led us to prepare a new activated sample of **1** (under the same conditions 353 K and 10^{-5} bar for 30 min) for a CO_2 sorption experiment performed at 196 K and 1 bar. Excitingly, this time the isotherm (showed in Figure 6) indicated a reversible CO_2 uptake of approximately

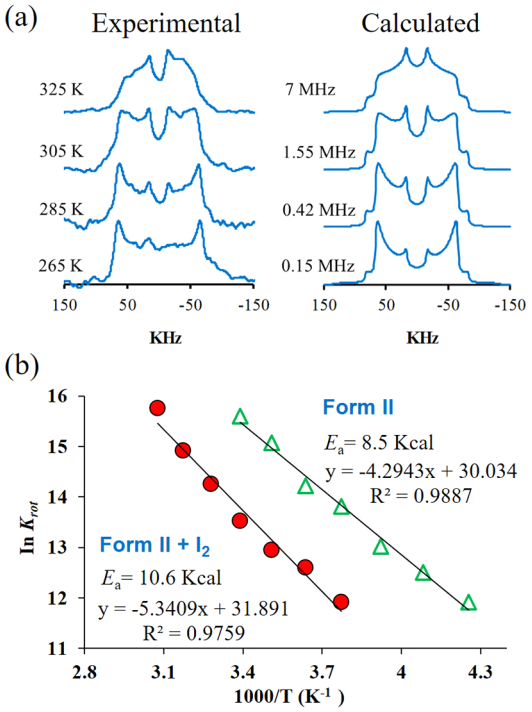

Figure 5. (a) Calculated and experimental ^{2}H line shapes from the solid exposed to I_2. (b) Arrhenius plots with and without chemical vapors.

Table 1. Comparison of the Activation Parameters from the Arrhenius and Eyring Plots

	E_a (kJ/mol)	A (s^{-1})	$\Delta H^{‡}$ (kJ/mol)	$\Delta S^{‡}$ (e.u.)
form II	35.5	1.1×10^{13}	33.5	−2.5
form II + I_2	44.3	7.0×10^{13}	41.9	12.0

DOI: 10.1021/jacs.7b02015
J. Am. Chem. Soc. 2017, 139, 7549–7557

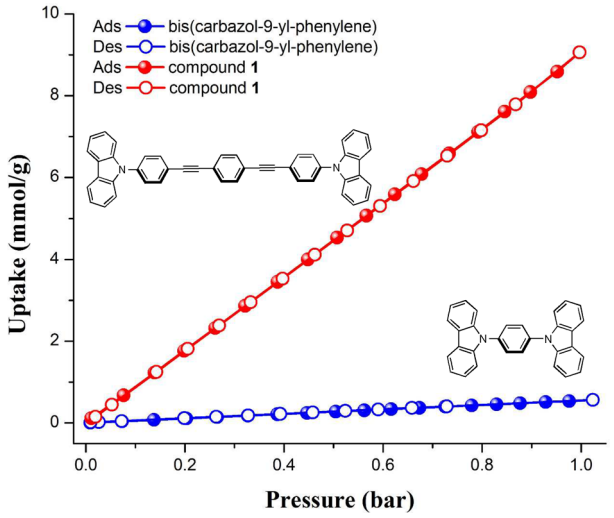

Figure 6. Adsorption (red solid circles) and desorption (red open circles) CO_2 isotherms for activated **1** compared to those of its shortest analog bis(carbazol-9-yl-phenylene) at 196 K.

9.0 mmol g^{-1}, with no hysteresis. The significant CO_2 uptake of **1** is 201.6 cm^3/g, that is, 4 times higher than the reported sorption for the porous rotor mentioned before[16] and comparable to tailored porous organic materials.[33] The uptake of **1** can even be compared to those exhibited by MOFs, with their characteristic permanent porosity due to their rigid walls and well-defined pores. For example, PCM-15[34] showed a CO_2 uptake of 14.1 mmol g^{-1}, with a BET surface area (calculated from its CO_2 adsorption at 196 K) of 1187 m^2 g^{-1}. Thus, we also estimated the surface area of activated **1** (*vide supra*), which was calculated from the CO_2 adsorption at 196 K to be 376 m^2 g^{-1}. The BET surface area of **1** is 2 times higher when compared to the permanently porous molecular rotor from the Sozzani group.

Subsequently, to corroborate the transient porosity of **1**, we decided to run two more cycles of CO_2 sorption experiments using the same sample but activating it between cycles (Figures S23 and S24). Remarkably, the adsorption−desorption isotherms exhibited the same reversible behavior and lack of hysteresis with total uptakes of 8.9 and 8.3 mmol g^{-1}, respectively. The average CO_2 uptake from the three sorption experiments was 8.7 mmol g^{-1}, and the corresponding BET surface area was 375.15 m^2 g^{-1}. It is noteworthy that after these CO_2 sorption experiments with cyclic measurements, the integrity of the solvent-free phase II was corroborated by the Rietveld refinement of its PXRD pattern (Figure S4). These results indicate that is possible to promote a transient porosity in this molecular rotor with a completely reversible process as confirmed by the CO_2 desorption. We attributed this high stability to the carbazole heterocycles, which in the rotor **1** act as anchors, producing highly robust molecular rotors.

Mechanism of the Transient Porosity in 1. Considering the sorption behavior and the surface area of **1**, which is approximately one-third that found in the porous PCM-15, it is remarkable to see that the CO_2 uptake of rotor **1** is not a third of that of MOF but quite higher. The high adsorption and the nonlinear behavior of the uptake versus surface area is not typically observed on rigid porous materials, so it seemed interesting to explore whether a correlation exists between the sorption behavior, the structure and the rotational dynamics. To do this, we carried out CO_2 sorption cycles at, 295, 273, 250, 231, 212, and 196 K along with solid-state ^2H NMR experiments (under N_2) at the same temperatures[35] (Figure 7).

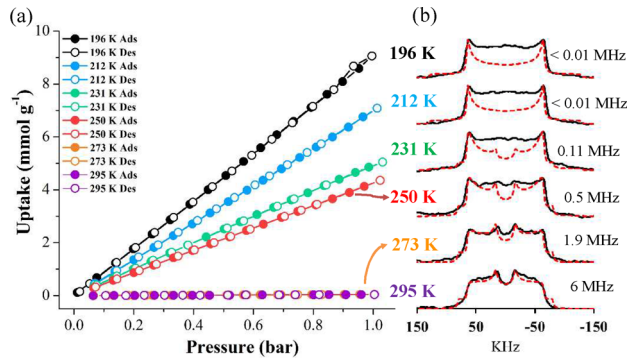

Figure 7. (a) Adsorption (solid circles) and desorption (open circles) CO_2 isotherms for activated **1**. (b) Experimental and simulated solid-state ^2H NMR line shapes at the same temperatures of the sorption experiments.

Comparable to the CO_2 adsorption−desorption isotherm at 196 K, the isotherms at 212, 231, and 250 K exhibited fully reversible CO_2 uptakes of approximately 7.1, 5.0, and 4.4 mmol g^{-1}, respectively at 1 bar, but at 273 and 295 K no significant adsorption was observed (Figure 7). The absence of hysteresis, in the experiments between 212 and 250 K, is consistent with the results of CO_2 adsorption−desorption experiment at 196 K. Interestingly, the CO_2 linear sorption that was clearly observed in all experiments here has been previously observed in MOFs. For example, PCM-14[36] exhibited a very similar linear correlation for the CO_2 adsorption. Conversely, the absence of hysteresis for **1** in the desorption step emphasizes the flexibility of **1**, as compared to that of PCM-14 which is a robust and rigid porous material that showed a marked hysteresis due to the strong interaction of CO_2 molecules with Ca(II) open metal sites.[36]

The isosteric CO_2 heat of adsorption (Q_{st}) for **1** was experimentally measured using two CO_2 isotherms (196 and 212 K) and the data were analyzed using a virial-type equation.[37] The value of $\ln(n/P)$ for a given amount adsorbed (n) was calculated by linear regression from the virial equation analysis (Figure S25). Thus, Q_{st} was equal to 15.4 kJ mol^{-1}, in good agreement with the value of the porous molecular rotor reported by the Sozzani group (21 kJ mol^{-1}).[16]

Regarding the intramolecular rotation, at 295 K the line shape that was best fitted to a 2-fold motion occurring at 6 MHz frequency. As the temperature gets lower, the line shape changes too, clearly reflecting the slowdown of the motion. Importantly, at 212 K and below, the experimental spectrum adopts the characteristic Pake pattern, suggesting that if any internal motion is present, it would take place at frequencies lower than 10^4 Hz. Since the CO_2 adsorption was increasingly higher at lower temperatures, it seems that the internal motion plays a role in the adsorption of CO_2. However, we think it is also important to consider that very high gas sorption could arise from the particularly flexible backbone of rotor **1**, which is based on soft ethynyl linkages that are easily bendable.[38]

Considering all the information, we postulate that the molecular flexibility and the lack of significant motion in **1** along with the relative pressure of CO_2 during the sorption experiments facilitate the gas molecules gradually going inside the crystalline sample at 196 K. Unfortunately, an *in situ* X-ray

DOI: 10.1021/jacs.7b02015
J. Am. Chem. Soc. 2017, 139, 7549−7557

study of the sample while performing the CO_2 sorption experiment was largely inaccessible. Instead, a visualization of the phenomenon was simulated, starting from the X-ray structure of **1** from synchrotron radiation and optimizing their geometries with two molecules of CO_2 inside. The simulations suggest that the CO_2 molecules could locate between the bent axes of **1** in this small cluster (Figure S26). To further support our argument, the shortest analog, bis(carbazol-9-yl)phenylene, a crystalline compound that has neither internal motion nor alkyne groups, was subjected to the same activation and sorption conditions and showed a negligible uptake (bottom of Figure 6).

Adsorption of Acetone. Encouraged by the CO_2 uptake results, we decided to evaluate the sorption capacity for solvent vapors. We explored several polar (acetone, acetonitrile, water, chloroform, ethanol, and methanol) and nonpolar solvents (benzene, hexane, and toluene) at 293 K. This temperature was chosen to avoid any solubility of compound **1** at higher temperatures (for example, 303 K).

The total uptakes for all the solvents were rather low (from approximately 0.4 to 1.2 wt %), except for acetone which shows a total uptake of 5.4 wt % (0.9 mmol g^{-1}) and a desorption hysteresis (Figure 8). The presence of acetone inside the

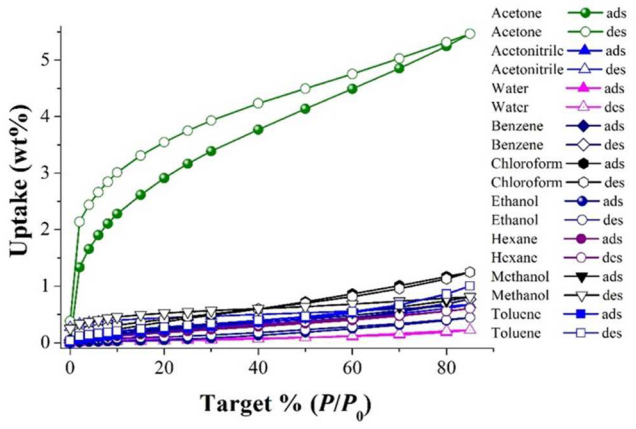

Figure 8. Vapor adsorption isotherms of compound **1** at 293 K and % P/P_0 = 0–85. Solid symbols represent adsorption and open symbols show desorption.

crystals of compound **1** was verified by FTIR (Figure S28), which showed a small band at 1715 cm^{-1}, corresponding to the C═O stretching, and no other significant changes were observed in the position of the bands. Using the new adsorption data, we went back to include acetone vapors in crystals of **1**-d_4 and acquire solid-state NMR (Figure S18). Gratifyingly, the fitting of the experimental ^2H line shape of the acetone-treated sample indicated a slightly slower internal motion of the central phenylene (0.6 MHz), as compared to the sample exposed to benzene vapors (0.7 MHz), verifying the larger acetone uptake with no phase changes (Figure S3). We propose that acetone accommodates not only within bent layers of **1** (Figure S27), but also via dipole interactions between the carbonyl group and the nitrogen atom from the carbazole group, giving rise to the hysteresis and reflecting the moderate physisorption between the relatively small and polar acetone vapor molecules and the carbazole heterocycles in compound **1**.

Indeed, the organic solvent uptake in **1** (ca. 0.9 mmol/g) is still lower than that found in a highly porous organic crystal reported recently (2.5 mmol/g),[39] although it was completely unanticipated in this dense crystal. Finally, we carried out a PXRD experiment after these vapor adsorption measurements, which confirmed the retention of the crystallinity of compound **1** (Figure S2). The vapor uptakes are in excellent agreement with the results of the dynamic characterization, indicating that only a small quantity of vapors is required to cause a slowdown of the rotational frequency as opposed to a fully reversible process that would completely stop the intramolecular rotation.

CONCLUSIONS

This work describes the solid-state ^2H NMR studies carried out to fully describe the internal dynamics of the molecular components in two crystal phases of rotor **1**. We have determined that benzene molecules contained inside the solvate (form I) experience rapid in-plane, 6-fold reorientations invisible to X-ray diffraction while acting as excellent stoppers for the internal rotation of compound **1**. When the benzene departures from the lattice, it triggers a phase transition that fully enables the motion of the rotator in **1**, which then adopts the thermally stable, solvent-free form II. Using the gel-assisted crystallization technique and synchrotron radiation, we obtained the X-ray structure of this form II, which is a densely packed organic crystal.

Interestingly, we have demonstrated that the rapid internal rotation in form II can be reduced by the diffusion of benzene or iodine vapors, which cause an increase of the E_a to rotation by 2 kcal/mol, as compared with that of the untreated crystalline solid. These findings led us to reveal the significant and selective CO_2 sorption properties of this seemingly nonporous rotor (201.6 cm^3 g^{-1}), with a SA_{BET} = 376 m^2 g^{-1}. The uptake was favored by the lack of internal motion at 196 K and the flexible *p*-(ethynylphenylene) backbone of the molecular rotor **1**, thus creating the mentioned transient pores. Thanks to the carbazole heterocycle that surrounds this axle, the same crystalline sample can endure cyclic experiments without losing its crystallinity. Finally, the sorption behavior using different solvents was also explored, with the larger uptake found when using acetone (5%), which also cause a reduction of the internal motion. Our work highlights the pivotal role of a rotary movement as an internal probe sensitive to guests. Work toward the development of other structurally conjugated compounds with similar behavior may be useful to obtain responsive materials with future applications and is currently underway.

ASSOCIATED CONTENT

Supporting Information

The Supporting Information is available free of charge on the ACS Publications website at DOI: 10.1021/jacs.7b02015.

Solid-state NMR spectra, single crystal and powder X-ray diffraction refinement details, DSC, TGA, sorption experiment details, EPR, X-ray fluorescence analyses (PDF)

Crystallographic information file for compound **1** (CIF)

AUTHOR INFORMATION

Corresponding Author

*E-mail: brodriguez@iquimica.unam.mx

ORCID

Elí Sánchez-González: 0000-0002-5440-329X

Ilich A. Ibarra: 0000-0002-8573-8033

DOI: 10.1021/jacs.7b02015
J. Am. Chem. Soc. 2017, 139, 7549–7557

Braulio Rodríguez-Molina: 0000-0002-1851-9957

Notes

The authors declare no competing financial interest.

■ ACKNOWLEDGMENTS

B.R.-M. thanks the financial support from CONACYT 238913. A. A.-G. thanks to CONACYT for a scholarship (279212). I.A.I. thanks the research funds from CONACYT (212318) and PAPIIT-UNAM (IN101517). The ALS is supported by the Director, Office of Science, Office of Basic Energy Sciences, U.S. Department of Energy, under contract no. DE-AC02-05CH11231. We acknowledge UCLA Department of Chemistry and Biochemistry for solid-state NMR. We thank for assistance Dr. Carmen García González (MS), M. Sc. Alejandra Nuñez Pineda (CCIQS, Thermal Analysis), Dr. Uvaldo Hernandez Balderas (CCIQS, PXRD), M. Sc. Virginia Gómez Vidales (EPR), María de los Ángeles Peña González, and M. Sc. Elizabeth Huerta Salazar (NMR). This research was partially supported by Laboratorio Nacional de Ciencias para la Investigación y Conservación del Patrimonio Cultural LANCIC Instituto de Fisica UNAM by CONACYT grants LN 232619, LN 260779, LN 271614, and LN 279740.

■ REFERENCES

(1) Litynski, J. T.; Klara, S. M.; McIlvried, h. G.; Srivastava, R. D. *Environ. Int.* **2006**, *32*, 128−144.

(2) Fuss, S.; Canadell, J. G.; Peters, G. P.; Tavoni, M.; Andrew, R. M.; Ciais, P.; Jackson, R. B.; Jones, C. D.; Kraxner, F.; Nakicenovic, N.; Le Quéré, C.; Raupach, M. R.; Sharifi, A.; Smith, P.; Yamagata, Y. *Nat. Clim. Change* **2014**, *4*, 850−853.

(3) Xu, Q., Ed. *Nanoporous materials: synthesis and applications*; CRC Press: Boca Raton, FL, 2013; pp 1−41.

(4) Das, S.; Heasman, P.; Ben, T.; Qiu, S. *Chem. Rev.* **2017**, *117*, 1515−1563.

(5) (a) Ricco, R.; Pfeiffer, C.; Sumida, K.; Sumby, C. J.; Falcaro, P.; Furukawa, S.; Champness, N. R.; Doonan, C. J. *CrystEngComm* **2016**, *18*, 6532−6542. (b) Tang, J.; Salunkhe, R. R.; Liu, J.; Torad, N. L.; Imura, M.; Furukawa, S.; Yamauchi, Y. J. *J. Am. Chem. Soc.* **2015**, *137*, 1572−1580.

(6) (a) Bandyopadhyay, S.; Anil, A. G.; James, A.; Patra, A. *ACS Appl. Mater. Interfaces* **2016**, *8*, 27669−27678. (b) Gu, S.; He, J.; Zhu, Y.; Wang, Z.; Chen, D.; Yu, G.; Pan, C.; Guan, J.; Tao, K. *ACS Appl. Mater. Interfaces* **2016**, *8*, 18383−18392. (c) Evans, J. D.; Huang, D. M.; Hill, M. R.; Sumby, C. J.; Sholl, D. S.; Thornton, A. W.; Doonan, C. J. *J. Phys. Chem. C* **2015**, *119*, 7746−7754.

(7) (a) Hasell, T.; Miklitz, M.; Stephenson, A.; Little, M. A.; Chong, S. Y.; Clowes, R.; Chen, L.; Holden, D.; Tribello, G. A.; Jelfs, K. E.; Cooper, A. I. *J. Am. Chem. Soc.* **2016**, *138*, 1653−1659. (b) Lu, X.; Jin, D.; Wei, S.; Wang, Z.; An, C.; Guo, W. *J. Mater. Chem. A* **2015**, *3*, 12118−12132. (c) Jin, Y.; Voss, B. A.; Jin, A.; Long, H.; Noble, R. D.; Zhang, W. *J. Am. Chem. Soc.* **2011**, *133*, 6650−6658.

(8) (a) Maina, J. W.; Pozo-Gonzalo, C.; Kong, L.; Schütz, J.; Hill, M.; Dumée, L. F. *Mater. Horiz.* **2017**, *4*, 345. (b) Haikal, R. R.; Soliman, A. B.; Amin, M.; Karakalos, S. G.; Hassan, Y. S.; Elmansi, A. M.; Hafez, I. H.; Berber, M. R.; Hassanien, A.; Alkordi, M. H. *Appl. Catal., B* **2017**, *207*, 347−357. (c) Guo, L.; Zeng, X.; Lan, J.; Yun, J.; Cao, D. *ChemistrySelect* **2017**, *2*, 1041−1047.

(9) (a) Tian, J.; Thallapally, P. K.; McGrail, B. P. *CrystEngComm* **2012**, *14*, 1909−1919. (b) Couderc, G.; Hulliger, J. *Chem. Soc. Rev.* **2010**, *39*, 1545−1554.

(10) (a) Lo Meo, P.; Lazzara, G.; Liotta, L.; Riela, S.; Noto, R. *Polym. Chem.* **2014**, *5*, 4499−4510. (b) Barbour, L. J. *Chem. Commun.* **2006**, 1163−1168. (c) Evans, J. D.; Huang, D. M.; Haranczyk, M.; Thornton, A. W.; Sumby, C. J.; Doonan, C. J. *CrystEngComm* **2016**, *18*, 4133−4141.

(11) (a) Hasell, T.; Cooper, A. I. *Nat. Rev. Mater.* **2016**, *1*, 16053. (b) Jiang, S.; Chen, L.; Briggs, M. E.; Hasell, T.; Cooper, A. I. *Chem. Commun.* **2016**, *52*, 6895−6898. (c) Burgun, A.; Valente, P.; Evans, J. D.; Huang, D. M.; Sumby, C. J.; Doonan, C. J. *Chem. Commun.* **2016**, *52*, 8850−8853. (d) Tian, J.; Thallapally, P. K.; Dalgarno, S. J.; McGrail, P. B.; Atwood, J. L. *Angew. Chem., Int. Ed.* **2009**, *48*, 5492−5495.

(12) (a) Tian, J.; Thallapally, P.; Liu, J.; Exarhos, G. J.; Atwood, J. L. *Chem. Commun.* **2011**, *47*, 701−703. (b) Couderc, G.; Hertzsch, T.; Behrnd, N.-R.; Krämer, K.; Hulliger, J. *Microporous Mesoporous Mater.* **2006**, *88*, 170−175. (c) Sozzani, P.; Bracco, S.; Comotti, A.; Ferretti, L.; Simonutti, R. *Angew. Chem., Int. Ed.* **2005**, *44*, 1816−1820. (d) Sozzani, P.; Comotti, A.; Simonutti, R.; Meersmann, T.; Logan, J. W.; Pines, A. *Angew. Chem., Int. Ed.* **2000**, *39*, 2695−2698.

(13) Herbert, S. A.; Janiak, A.; Thallapally, P. K.; Atwood, J. L.; Barbour, L. J. *Chem. Commun.* **2014**, *50*, 15509−15512.

(14) (a) Ananchenko, G.; Moudrakovski, I. L.; Coleman, A. W.; Ripmeester, J. A. *Angew. Chem., Int. Ed.* **2008**, *47*, 5616−5618. (b) Holden, D.; Chong, S. Y.; Chen, L.; Jelfs, K.; Hasell, T.; Cooper, A. I. *Chem. Sci.* **2016**, *7*, 4875−4879.

(15) (a) Dron, P. I.; Zhao, K.; Kaleta, J.; Shen, Y.; Wen, S.; Shoemaker, R. K.; Rogers, C. T.; Michl, J. *Adv. Funct. Mater.* **2016**, *26*, 5718−5732. (b) Catalano, L.; Perez-Estrada, S.; Wang, H.-H.; Ayitou, A. J.-L.; Khan, S. I.; Terraneo, G.; Metrangolo, P.; Brown, S.; Garcia-Garibay, M. A. *J. Am. Chem. Soc.* **2017**, *139*, 843−848. (c) Masuda, T.; Arase, J.; Inagaki, Y.; Kawahata, M.; Yamaguchi, K.; Ohhara, T.; Nakao, A.; Momma, H.; Kwon, E.; Setaka, W. *Cryst. Growth Des.* **2016**, *16*, 4392−4401. (d) Aprahamian, I. *Nat. Chem.* **2015**, *8*, 97−99. (e) Colin-Molina, A.; Pérez-Estrada, S.; Roa, A. E.; Villagrana-Garcia, A.; Hernández-Ortega, S.; Rodríguez, M.; Brown, S. E.; Rodríguez-Molina, B. *Chem. Commun.* **2016**, *52*, 12833−12836. (f) Comotti, A.; Bracco, S.; Sozzani, P. *Acc. Chem. Res.* **2016**, *49*, 1701−1710.

(16) Comotti, A.; Bracco, S.; Yamamoto, A.; Beretta, M.; Hirukawa, T.; Tohnai, N.; Miyata, M.; Sozzani, P. *J. Am. Chem. Soc.* **2014**, *136*, 618−621.

(17) (a) Dong, J.; Tummanapelli, A. K.; Li, X.; Ying, S.; Hirao, H.; Zhao, D. *Chem. Mater.* **2016**, *28*, 7889−7897. (b) Kanoo, P.; Haldar, R.; Reddy, S.; Hazra, A.; Bonakala, S.; Matsuda, R.; Kitagawa, S.; Balasubramanian, S.; Maji, T. K. *Chem. - Eur. J.* **2016**, *22*, 15864−15873. (c) Horike, S.; Matsuda, R.; Tanaka, D.; Matsubara, S.; Mizuno, M.; Endo, K.; Kitagawa, S. *Angew. Chem., Int. Ed.* **2006**, *45*, 7226−7230. (d) Khudozhitkov, A. E.; Jobic, H.; Freude, D.; Haase, J.; Kolokolov, D. I.; Stepanov, A. G. *J. Phys. Chem. C* **2016**, *120*, 21704−21709. (e) Kolokolov, D. I.; Jobic, H.; Stepanov, A. G.; Guillerm, V.; Devic, T.; Serre, C.; Férey, G. *Angew. Chem., Int. Ed.* **2010**, *49*, 4791−4794.

(18) (a) Bracco, S.; Beretta, M.; Cattaneo, A.; Comotti, A.; Falqui, A.; Zhao, K.; Rogers, C.; Sozzani, P. *Angew. Chem., Int. Ed.* **2015**, *54*, 4773−4777. (b) Vogelsberg, C.; Bracco, S.; Beretta, M.; Comotti, A.; Sozzani, P.; Garcia-Garibay, M. A. *J. Phys. Chem. B* **2012**, *116*, 1623−1632. (c) Comotti, A.; Bracco, S.; Valsesia, P.; Beretta, M.; Sozzani, P. *Angew. Chem., Int. Ed.* **2010**, *49*, 1760−1764.

(19) Blanc, F.; Chong, S. Y.; McDonald, T. O.; Adams, D. J.; Pawsey, S.; Caporini, M. A.; Cooper, A. I. *J. Am. Chem. Soc.* **2013**, *135*, 15290−15293.

(20) Comotti, A.; Bracco, S.; Mauri, M.; Mottadelli, S.; Ben, T.; Qiu, S.; Sozzani, P. *Angew. Chem.* **2012**, *124*, 10283−10287.

(21) Aguilar-Granda, A.; Pérez-Estrada, S.; Roa, A. E.; Rodríguez-Hernández, J.; Hernández-Ortega, S.; Rodriguez, M.; Rodríguez-Molina, B. *Cryst. Growth Des.* **2016**, *16*, 3435−3442.

(22) Duer, M. J. *Introduction to Solid-State NMR Spectroscopy*; Blackwell: Oxford, U.K., 2004; pp 293−330.

(23) Macho, V.; Brombacher, L.; Spiess, H. W. *Appl. Magn. Reson.* **2001**, *20*, 405−432.

(24) (a) Hughes, C. E.; Harris, K. D. M. *Chem. Commun.* **2010**, *46*, 4982−4984. (b) Hughes, C. E.; Harris, K. D. M. *J. Phys. Chem. A* **2008**, *112*, 6808−6810.

(25) (a) Albunia, A. R.; Graf, R.; Grassi, A.; Guerra, G.; Spiess, H. W. *Macromolecules* **2009**, *42*, 4929−4931. (b) Masierak, W.; Emmler, T.;

DOI: 10.1021/jacs.7b02015
J. Am. Chem. Soc. 2017, 139, 7549−7557

Gedat, E.; Schreiber, A.; Findenegg, G. H.; Buntkowsky, G. *J. Phys. Chem. B* **2004**, *108*, 18890−18896.
(26) Horike, S.; Shimomura, S.; Kitagawa, S. *Nat. Chem.* **2009**, *1*, 695−704.
(27) (a) Rizzato, S.; Moret, M.; Merlini, M.; Albinati, A.; Beghi, F. *CrystEngComm* **2016**, *18*, 2455−2462. (b) Sharninghausen, L. S.; Mercado, B. Q.; Crabtree, R. H.; Balcells, D.; Campos, J. *Dalton Trans.* **2015**, *44*, 18403−18410. (c) Mahieux, J.; Sanselme, M.; Coquerel, G. *Cryst. Growth Des.* **2013**, *13*, 908−917. (d) Pietras, Z.; Lin, H.-T.; Surade, S.; Luisi, B.; Slattery, O.; Pos, K. M.; Moreno, A. *J. Appl. Crystallogr.* **2010**, *43*, 58−63. (e) Oaki, Y.; Imai, H. *Cryst. Growth Des.* **2003**, *3*, 711−716.
(28) Takahashi, Y.; Tadokoro, H. *Macromolecules* **1973**, *6*, 672−675.
(29) The same solution was obtained when the crystals were collected using the X-ray diffractometer with Cu Kα1 radiation, although the R_1 value was considerably larger (22%).
(30) (a) Yun, W. J.; Cho, J. M.; Lee, J.-K. *Synth. Met.* **2006**, *156*, 848−851. (b) Brinkmann, M.; Videva, V. S.; Bieber, A.; André, J. J.; Turek, P.; Zuppiroli, L.; Bugnon, P.; Schaer, M.; Nuesch, F.; Humphry-Baker, R. *J. Phys. Chem. A* **2004**, *108*, 8170−8179. (c) Lüssem, B.; Keum, C.-M.; Kasemann, D.; Naab, B.; Bao, Z.; Leo, K. *Chem. Rev.* **2016**, *116*, 13714−13751.
(31) Kamaruzaman, D.; Ahmad, N.; Annuar, I.; Rusop, M. *Jpn. J. Appl. Phys.* **2013**, *52*, 11NL02−8.
(32) (a) Yan, Z.; Yuan, Y.; Tian, Y.; Zhang, D.; Zhu, G. *Angew. Chem., Int. Ed.* **2015**, *54*, 12733−12737. (b) Pearson, A. J.; Xiao, W. *J. Org. Chem.* **2003**, *68*, 5361−5368.
(33) (a) Hisaki, I.; Nakagawa, S.; Ikenaka, N.; Imamura, Y.; Katouda, M.; Tashiro, M.; Tsuchida, H.; Ogoshi, T.; Sato, H.; Tohnai, N.; Miyata, M. *J. Am. Chem. Soc.* **2016**, *138*, 6617−6628. (b) Hisaki, I.; Nakagawa, S.; Tohnai, N.; Miyata, M. *Angew. Chem., Int. Ed.* **2015**, *54*, 3008−3012.
(34) Ibarra, A.; Hesterberg, T. W.; Holliday, B. J.; Lynch, V. M.; Humphrey, S. M. *Dalton Trans.* **2012**, *41*, 8003−8009.
(35) The new ^{2}H experiments were acquired at 92 MHz frequency.
(36) Ibarra, I. A.; Tan, K. E.; Lynch, V. M.; Humphrey, S. M. *Dalton Trans.* **2012**, *41*, 3920−3923.
(37) (a) Zhao, X.; Villar-Rodil, S.; Fletcher, A. J.; Thomas, K. M. *J. Phys. Chem. B* **2006**, *110*, 9947−9955. (b) Ibarra, I. A.; Mace, A.; Yang, S.; Sun, J.; Lee, S.; Chang, J.-S.; Laaksonen, A.; Schröder, M.; Zou, X. *Inorg. Chem.* **2016**, *55*, 7219−7228.
(38) (a) Schwab, P. F. H.; Levin, M. D.; Michl, J. *Chem. Rev.* **1999**, *99*, 1863−1934. (b) Godt, A.; Schulte, M.; Zimmermann, H.; Jeschke, G. *Angew. Chem., Int. Ed.* **2006**, *45*, 7560−7564.
(39) Sheng, Y.; Chen, Q.; Yao, J.; Lu, Y.; Liu, H.; Dai, S. *Angew. Chem.* **2016**, *128*, 3439−3442.

DOI: 10.1021/jacs.7b02015
J. Am. Chem. Soc. 2017, 139, 7549−7557